A comparison of flow boiling heat-transfer in in-line mini pin fin and plane channel flows

D.A. Mcneil, A.H. Raeisi, P.A. Kew, P.R. Bobbili

Accepted Manuscript

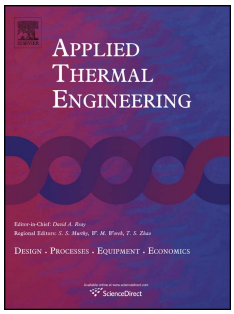

Title: A comparison of flow boiling heat-transfer in in-line mini pin fin and plane channel flows

Authors: D.A. McNeil, A.H. Raeisi, P.A. Kew, P.R. Bobbili

PII: S1359-4311(10)00258-9

DOI: 10.1016/j.applthermaleng.2010.06.011

Reference: ATE 3142

To appear in: *Applied Thermal Engineering*

Received Date: 22 December 2009

Revised Date: 2 June 2010

Accepted Date: 14 June 2010

Please cite this article as: D.A. McNeil, A.H. Raeisi, P.A. Kew, P.R. Bobbili. A comparison of flow boiling heat-transfer in in-line mini pin fin and plane channel flows, Applied Thermal Engineering (2010), doi: 10.1016/j.applthermaleng.2010.06.011

ABSTRACT:

The use of a boiling fluid as a coolant is an attractive option for electronic devices as electrical power densities increase. However, for systems working at the micro-scale, design methods developed for evaluating heat transfer in macro-scale evaporators are not appropriate for passages with hydraulic diameter of the order of 1mm and below.

Heat-transfer coefficients and pressure drops are reported for two surfaces, a pin-fin and a plate surface, each with 50 mm square base area. The pin-fin surface was comprised of 1 mm square pin-fins that were 1mm high and located on a 2 mm square pitch array covering the base. The channel was 1 mm high and had a glass top plate. The data were produced while boiling R113 at atmospheric pressure. For both surfaces, the mass flux range was 50 -250 kg/m^{2}s and the heat flux range of 5-140 kW/m^2. The results obtained have been compared with a standard correlation for tube bundles.

The measured heat transfer coefficients for the pin-fin surface are slightly higher than those for the plate surface. Both are dependent on heat flux and reasonably independent of mass flux and vapour quality. Thus, heat transfer is probably dominated by nucleate-boiling and is increased by the pin-fins due to the increase in area and heat-transfer coefficient. The pin-fin pressure drops were typically 7 times larger than the plate values.

The pin-fin heat-transfer coefficients and pressure drops are compared to macro-scale tube bundle correlations. At low vapour qualities the heat-transfer coefficients are in reasonable agreement with the correlations, but, as the vapour quality increases, they do not show the convective enhancement which would be expected for a conventionally-sized tube bundle. Measured two–phase pressure drops are in reasonable agreement with the tube bundle correlation.

A comparison of flow boiling heat-transfer in in-line mini pin fin and plane channel flows

D A McNeil*, A H Raeisi , P A Kew and P R Bobbili

Department of Mechanical Engineering

Heriot-Watt University

Edinburgh EH14 4AS

***corresponding author D.A.McNeil@hw.ac.uk**

Key words: Boiling, pin-fins, mini-scale, pressure drop

1. Introduction

In recent years, electronic devices, such as micro-processors and lasers, have increased in power consumption and reduced in physical size. This has led to an increasing intensity in heat generation that needs to be removed during normal operation. Removing heat is becoming increasingly difficult. It therefore seems likely that new methods will be needed in the not too distant future. One possibility is to use a boiling fluid as the coolant, as this would transfer significantly more heat than its single-phase equivalent. This has led to an abundance of research into boiling in small diameter channels.

It has been demonstrated that there is a length scale, below which, methods derived for large diameter tubes are no longer appropriate. What is less clear is what that length scale should be. For a two-phase mixture flowing in a channel of hydraulic diameter D_h, Kew and Cornwell (1997) defined the Confinement number, Co, as

$$Co = \left[\frac{\sigma}{g(\rho_L - \rho_V) D_h^2} \right]^{1/2} \quad (1)$$

where g is the acceleration due to gravity, σ is the surface tension and ρ_L and ρ_V are the liquid and vapour densities respectively. They showed that when $Co > 0.5$, macro-scale methods could be applied, otherwise micro-scale methods had to be used. Other researchers have claimed that three length scales are needed, macro, mini and micro. Mehendal et al. (2000) classified the channels through the hydraulic diameter. Micro-channels occurred in the range 1-100 μm, mini-channels in the range 100-1000 μm and macro-channels at values grater than 1 mm. Kandlikar (2001) took a similar approach, classifying micro-channels in the range 50-600 μm, mini-channels in the range

600-3000 μm and macro-channels channels at values greater than 3 mm. The change from methods valid at the macro-scale to those valid at the micro-scale results from a change in the controlling forces, for example, gravity forces becoming less important than surface tension forces. It thus seems unlikely that hydraulic diameter ranges will prove to be universal. An approach similar to that taken by Kew and Cornwell (1997) seems more likely to lead to a universal classification. Kew et al (2006) have shown that the Confinement number is also applicable to more complex geometries.

A number of studies have been undertaken for single tubes, e.g. Lazarek and Black (1982), Wambsganss and co workers (1993, 1996), Lin et al (2001), Thome et al (2004) and Shiferaw et al (2009). Several studies have attempted to correlate the heat-transfer coefficient by modifying the macro-scale correlations. These approaches divide the heat transfer into nucleate and convective boiling components. The results produced are complex and cannot be used with confidence, see for example Zhang et al (2004) and Kandlikar and Steinke (2002). More recent works recognise the importance of flow pattern. For example, the three zone model of Thome et al (2004) has been shown to be applicable in the absence of dryout. However, the model of Kew and Cornwell (1997), developed by Yan and Kenning (1998), demonstrates that expanding confined bubbles accelerate liquid slugs, causing pressure fluctuations and intermittent dryout at relatively low qualities. Similar instabilities have been observed by Barber et al (2009). Neither of these phenomena is included in the three zone model. Thus, a comprehensive understanding of micro-scale boiling in single channels has yet to be attained.

Work on multiple parallel micro-channels has revealed the importance of instabilities that result in flows with different flow patterns appearing in different tubes simultaneously, Hestroni et al (2003). Qu and Mudawar (2003) concluded that existing correlations for boiling in single micro-channels were not applicable to multi-channel arrangements. Several instabilities have been identified. Xu et al (2005), working with water and methanol in 26 parallel rectangular channels 0.3 mm x 0.8 mm x 50 mm long, classified the instabilities in terms of duration. Large amplitude/long period oscillations, occurring at 117 s intervals, resulted in large pressure pulses, with smaller oscillations occurring at periods of the order of a 10 s. Wang et al (2007) boiled water in 8 parallel channels that were 30 mm long with a hydraulic diameter of 0.186 mm. Two instabilities were observed, one with periods of 3-7 s, increasing with decreasing mass flux, and one with a period of 0.1 s. Bogojevic et al (2009) used 40 parallel channels

15 mm long with a hydraulic diameter of 0.194 mm. Again two frequency ranges were observed, one with periods greater than 0.3 s and one with a period of 0.04 s, with the dominant instability being dependent upon the heat- to mass-flux ratio.

For boiling in complex geometries, many studies have been undertaken at the macro-scale. For example, for tube bundles, Shrage et al (1988), Dalwati et al (1990, 1992) and Feenstra et al (2000) have investigated void fraction distributions, while Ishihara et al (1980), proposed a method for the frictional two-phase multiplier. Fewer studies have been undertaken at the micro-scale. A review of various surface enhancement methods, including drilled cavities, re-entrant cavities, alumina sprayed particles and microstructures, has been reported by Honda and Wei (2004) for nucleate boiling heat transfer. The key issues identified were the temperature overshoot required to initiate boiling, the effect of liquid subcooling and the critical heat flux. The overshoot temperature is shown to decrease with increased roughness of the microstructure. However, the most effective method of reducing temperature overshoot was gasification of the liquid. This could allow boiling below the saturation temperature and had little effect on the performance at high, or near critical, heat flux. Honda and Wei (2004) also reported that the heat transfer and critical heat flux were found to improve with enhanced area, but not in direct proportion. Critical heat flux was found to increase with increasing subcooling. The most effective enhancement method was found to be pin fins. This gave enhanced heat transfer because vapour trapped between the fins provided additional nucleation sites. Additionally, these spaces retained vapour for longer, giving enhanced heat transfer. The optimum spacing of the fins depended on liquid subcooling.

Honda et al (2002) undertook nucleate boiling studies, from free convection up to critical heat flux, on a pin-fin array using FC-72 at atmospheric pressure as the working fluid. The pin-fins were 50 μm square, 60 μm high and were ordered in an in-line, square pitch configuration with a 100 μm pitch. The test piece was 10 mm square. Heat fluxes of up to 620 kW/m^2 were used with liquid subcoolings of up to 45 ^{o}C. The additional fin area was not included in the calculation of the heat-transfer coefficient. In the free convection region, for the same wall-to-fluid temperature difference, the pin fins had a lower heat flux than a flat surface, despite having an area enhancement of 2.2. This was because the pin fins lay below the thermal boundary layer. At higher temperature differences, the pin-fins produced heat fluxes up to 1.8 times larger and a greater critical heat flux. The rapid growth in heat flux was caused by vapour

trapped between the pin fins. The bubbles grew to many times the volume of a pin fin and, at critical heat flux, the surface was covered with very large bubbles. When dissolved gas was included, boiling was observed at negative saturation-to-wall temperature differences.

Lie et al (2007) investigated flow boiling of FC-72 on plain and pin finned surfaces at atmospheric pressure. Two pin-fin surfaces were tested, one with fins 200 μm square and 70 μm high on a square in line arrangement with a 400 μm pitch, and one with fins 100 μm square and 70 μm high on a square in-line arrangement with a 200 μm pitch. The mass fluxes used were within the range 287-431 kg/m^{2}s and the heat fluxes within 1-100 kW/m^2. Single-phase and flow boiling heat transfer coefficients were reported. The single-phase, heat-transfer coefficients were based on the mean-wall to fluid-inlet temperature difference and the base area of the heat-transfer surface. The boiling coefficients used the mean-wall to fluid-saturation temperature difference. The mass flux was found to have only a slight effect on the boiling heat-transfer coefficient. The temperature at the onset of nucleate boiling was found to increase with increasing mass flux and, for the same temperature difference, the largest heat transfer occurred with the 100 μm fins. Cross-flow between channels was evident. The degree of wall superheat required for the onset of boiling was lower for the finned surfaces, with increased nucleation sites being evident in the corners of the fins. Bubbles grew to many times the size of the fins and became elongated and distorted. The bubble departure diameter reduced with increasing mass flux and with the addition of fins. The departure frequency increased with mass flux and the addition of fins. Correlations of the heat-transfer coefficients were produced by assuming that a convective and boiling component of heat flux existed.

Kosar and Peles (2007) investigated flow boiling using micro pin-fins manufactured as NACA 66-021 hydrofoils. The fins were in a staggered arrangement with 12 or 13 fins lateral to the flow on a lateral pitch of 150 μm and 20 fins in the flow direction with a pitch of 500 μm. Each fin had a chord length of 100 μm, a length of 500 μm, a wetted perimeter of 1.03 mm and a height of 243 μm. The working fluid was R123 at pressures between 486-539 kN/m^2. The experiments were conducted by setting the mass flow rate and increasing the voltage to the heater in steps of 1 V until critical heat flux occurred. The fluid entered the test section in a subcooled state. The test-section was split into single and two-phase lengths from the video record. The exit quality was obtained from a heat balance. Single-phase, partial boiling and fully-developed boiling ranges were identified. Average heat-transfer coefficients

were deduced using the fin-efficiency concept. The single-phase heat-transfer coefficient was found to vary from 4.8 to 15.5 kW/m^{2}K in the mass flux range 972-2349 kg/m^{2}s via a power law relationship with an exponent of 0.75. The boiling heat-transfer coefficient was found to increase in the assumed nucleate boiling region and decease in the assumed convective boiling region to critical heat flux. Critical heat flux was therefore due to the dryout mechanism. The bubbly, wavy intermittent and spray-annular flow patterns were identified. Nucleate boiling heat transfer was associated with the bubbly and wavy intermittent flow patterns while convective boiling was associated with the spray-annular flow pattern. The measured boiling data were not well predicted by macro-channel methods. The critical heat flux increased with mass flux, decreased with exit quality and was reasonably well predicted from micro-channel methods.

Kosar (2008), working on the same test facility as Kosar and Peles (2007), reported single and two-phase pressure drops for the hydrofoil test piece. For a set mass flux, the pressure drop reduced at low heat fluxes due to the reduced viscosity of the fluid, while at higher heat fluxes, after the onset of significant vapour generation, the pressure drop increased. Pressure drop increased with mass flux and with gas-mass fraction for the same mass flux. Thus, for the same heat flux, a lower mass flux could have a larger pressure drop than a larger one because of the larger exit gas-mass fraction. A Chisholm type fit was attempted to the two-phase friction multiplier, deduced from the pressure-drop measurements using the laminar-laminar flow combination Martinelli parameter, X_{vv}. The correlation was poor. The flow map transition from bubbly to wavy intermittent flow was found to occur when X_{vv} was 1.8 and the transition from wavy-intermittent to spray annular occurred when X_{vv} was 3.

Krishnamurthy and Peles (2008) reported flow boiling in circular pin fins with water at atmospheric pressure. The fins had a diameter of 100 μm and a height of 250 μm and were placed in a staggered configuration with a pitch of 150 μm. There were 11 or 12 columns and 68 rows. Orifice plates were placed upstream of the test piece to suppress thermo-hydraulic instabilities. Tests were carried out by setting a constant mass flux between 346 and 794 kg/m^{2}s and increasing the voltage to the heater in steps of 0.5 V until critical heat flux occurred. The average wall temperature was derived from the heater resistance. Local thermistors allowed the local heat-transfer coefficient to be deduced using the fin efficiency approach and assuming no heat transfer from the fin tips. At all but the highest mass flux, single-phase heat transfer progressed to fully developed boiling. At the highest heat flux these regimes

were separated by a partial boiling regime. The partial boiling regime was caused by large vapour slugs on the test piece preceding annular flow. The single-phase heat-transfer coefficient was found to be proportional to the mass flux. The two-phase heat-transfer coefficient was found to vary moderately with mass flux and to be independent of heat flux, suggesting convective boiling domination. A Chen type correlation was deduced by neglecting the nucleate boiling component and applying a Reynolds analogy, for which a single-phase coefficient proportional to a one third power law with mass flux was used. Only the slug and annular flow patterns were observed.

Ma et al (2009) investigated flow boiling of FC-72 at atmospheric pressure on square pin finned arrays. The fins were 30 μm wide and arranged on a square in-line configuration with a pitch of 60 μm. Two fin heights of 60 μm and 120 μm were tested. Both were compared to an open channel, or smooth, flow. The test pieces were 10 mm square and 0.5 mm high and were placed in a flow channel 30 mm wide and 5 mm high. The test piece location was 300 mm from the flow inlet. The downstream flow length was longer. The channel flow characteristics were therefore not affected by the thermo-hydraulics of the test piece. The FC-72 liquid was saturated with air to prevent overshot at the onset of boiling. Channel liquid velocities of 0.5, 1 and 2 m/s were tested at inlet subcoolings of 15, 25 and 35 K. Tests were carried out by increasing the Joule heating in steps until critical heat flux occurred. The smooth test piece showed the critical heat flux to increase with both liquid velocity and subcooling. The fin area was not corrected for in the heat transfer analysis. For the same wall-fluid temperature difference, the single and two-phase heat fluxes were significantly enhanced by the addition of fins and an increase in fin height. Boiling heat-transfer was enhanced by increased nucleation in the gaps between the fins. At liquid velocities of 0.5 and 1 m/s, the two-phase heat flux varied as a power law of the temperature difference, while at 2 m/s, it varied linearly. This suggested that nucleate boiling and forced convective heat transfer were important. Critical heat flux increased with liquid velocity, subcooling and the addition of fins. Yuan et al (2009) reported very similar work with a fin width of 50 μm on a 100 μm pitch. The conclusions were very similar.

Qu and Siu-Ho (2009) investigated water boiling at atmospheric pressure in a square pin fin array. The test piece was 33.8 mm long and 10 mm wide and contained 1950 fins 200 μm wide and 670 μm high on a staggered configuration with a lateral and transverse pitch of 400 μm. The ratio of the total to the base area was 3.9. Fin efficiency was used to include the pin fin areas in the heat-transfer analysis. Water with mass fluxes of 183-420 kg/m^{2}s and with

subcoolings of 10, 40 and 70 K were supplied to the test piece. Three in wall thermocouples allowed local heat-transfer coefficients to be deduced. Partitioning the test piece into subcooled and saturated liquid portions from a heat balance allowed single and two-phase heat transfer to be identified. Only the saturated heat-transfer coefficients obtained at exit gas-mass fractions greater than 0.01 were reported. The saturated boiling values had unusual characteristics, being insensitive to mass flux and heat flux, but not exit quality. The observed flow pattern was said to be annular which suggested that the boiling heat-transfer mechanism was convective. The lack of mass flux dependency was explained in terms of a constant liquid film induced by the pin fins, and subcooled entrained liquid. The data were correlated in terms of an 'equilibrium' heat transfer coefficient and the exit gas-mass fraction.

Krishnamurthy and Peles (2009) reported on an adiabatic study of nitrogen-ethanol flows across a staggered array of circular pin fins. The test piece was 1.5 mm wide and 10 mm long and contained 68 rows of fins in either 9 or 10 columns. The fins were 10 μm in diameter and 10 μm high and were configured in a staggered array with a longitudinal and transverse pitch of 150 μm. Surface tension effects were deduced by comparing the results from a previous study, Krishnamurthy and Peles (2007), where water was used. Water has a similar density and viscosity to ethanol but a much higher surface tension. High speed photography was used to inspect the flow pattern and to determine the void fraction at several locations in the transverse direction. The void fraction was reasonably independent of transverse position, indicating that the flow became fully developed after a few rows of fins. Except for a small range of gas-mass fractions, the void fraction was found to be reasonably independent of surface tension, allowing their (2007) correlation to be used. The flow pattern transition boundaries were found to depend on surface tension. The pressure drop was also affected because of its flow map dependence. A modified Chisholm type correlation was produced for the two-phase multiplier. An interfacial friction factor was deduced using methods similar to Rahman et al. (1996).

Macro sized heat exchangers typically have tubes 20 mm in diameter on an in-line or staggered arrangement with a pitch to diameter ratio of about 1.5. Micro pin fins in the range 30-200 μm in diameter on in-line and staggered arrangements have been investigated. Nothing has been reported in between. The objective of this study is to investigate flow boiling in a complex geometry at an intermediate size. Thus, this study was undertaken to obtain heat-transfer and pressure drop data for a surface containing square pin fins 1 mm wide and 1 mm high placed in an

in-line arrangement on a 2 mm pitch, and to compare them with similar data obtained for a flat plate surface. The data were obtained using R113 at atmospheric pressure.

2. Description of the test facility

The flow loop is shown schematically in Fig. 1. Liquid R113 was drawn from the accumulator by the diaphragm pump. Valves in the by-pass and main lines allowed the desired mass flow rate to be set. Liquid passed from the pump to a filter. The coarse filter was used initially to remove large debris. The finer filter was used during testing. Liquid passed from the filter to a Micro-motion, coriollis, mass-flow meter, where the liquid flow rate was measured to within 0.1% of reading. From the flow meter, the liquid passed through a pre-heater, where the its temperature was set to obtain a subcooling of between 2-5 ^{o}C, before it passed through a sight glass, where visual observation confirmed a liquid entry to the test section. Boiling occurred in the test section. Sheathed, K-type thermocouples were located upstream and downstream to allow the inlet and outlet temperatures to be measured. High speed videos were taken of the boiling occurring on the test piece by a Kodak micromotion 1000 camera. The camera was set to 240 frames/s at a resolution of 720 by 480 pixels. Fluid from the test section passed to a t-piece, where the liquid and vapour were separated. The vapour moved vertically upwards and was condensed in the condenser before being re-united with the separated liquid that had moved vertically downwards. The re-united liquid flow passed through a sub-cooler before returning to the accumulator.

The test section is shown in Fig. 2. Liquid entered the volume chamber of the test-section through the two inlet ports, set at 90^{o} to the direction of flow in the test piece. The volume chamber dimensions were set to reduce the liquid velocity to close to zero before it accelerated into the settling length upstream of the test piece, Fig. 2b. Pressure tappings were located just upstream and downstream of the test piece. The liquid pressure was measured at the upstream tapping with a 0-12 bar absolute pressure transducer, accurate to 0.2% of reading. The pressure difference across the tappings was measured with a Rosemount differential pressure transducer, model 3051C. This was a smart transducer that allowed the pressure drop range to be set prior to testing. The transducer was accurate to ±0.25% of reading. The fluid boiled as it passed across the test piece. Heat was supplied to the test section from a Wattlow Ultramic ceramic heater. The heater was 50 mm square

and was placed below the test piece. The heater was fixed to the test section by a securing plate, Fig. 2c. A PTFE block was located between the securing plate and the heater to minimize heat transfer from the lower surface of the heater. Power to the heater was adjusted to give the required heat flux. The heat load was measured with a RS wattmeter to 1% of reading.

The pin-fin test piece is shown in Fig. 3. It was constructed from a piece of copper, 50 mm wide by 50 mm long and 6 mm high. The complex geometry was formed by cutting slots 1 mm wide and 1 mm deep in the longitudinal and transverse directions. The slots were 1 mm apart. Three holes, 0.6 mm in diameter by 12.5 mm long, were drilled into the test piece at the inlet and outlet ends. The holes were located 2.5 mm from the top of the boiling surface and 11, 25 and 39 mm from an edge. These holes allowed six sheathed K-type thermocouples, 0.5 mm in diameter, to be located below the boiling surface. All thermocouples were calibrated in a water bath and were accurate to ±0.1 K. The plate test piece had similar overall dimensions, i.e. the plate layout corresponds to the pin-fin test piece with the pins removed.

The thermocouples were connected to a NI 9211 thermocouple differential unit connected to a NI 9172 data acquisition system. The pressure transducers and the flow meter were connected to an NI 9205 system. Both systems were connected to a PC and controlled with Labview software. The thermocouple, pressure, pressure drop and mass flow readings were obtained over a 40 s period, during which 2000 readings of each were obtained. This gave reproducible average values for all.

The fluid was boiled vigorously for 2 hours before a test series. During this period the vent valve above the condenser was periodically opened to allow dissolved gases to escape to the atmosphere. This also set the test pressure to near atmospheric.

Tests were conducted by setting the required liquid flow rate. The pre-heater was attached to a controller. The controller was set to the required temperature before the pre-heater was switched on. The liquid was circulated through the flow loop until the required entry temperature was achieved. This took approximately one hour. The test section was then set to the desired heat flux. Steady state conditions were achieved when the fluid

outlet and the aluminium body temperatures were shown to be stable. This took approximately 35-40 minutes. All of the required readings were obtained before the heat flux was re-set to the next desired value and the process repeated.

3. Heat losses in the test-section

The test section was designed to operate at pressures of up to 10 bar. Thus, the aluminium body had significant thickness that allowed several heat paths to exist from the heater to the fluid. The conduction heat paths were simulated using Ansys CFX 11 software. The test section was meshed as a multi-domain body, allowing the appropriate thermal conductivity to be entered for each material in the test section. 800,000 finite volumes were used. A constant heat flux boundary condition was assumed at the heater. Heat-transfer coefficient with temperature boundary conditions were assumed at all fluid-solid boundaries. If the boundary was solid-liquid, the heat-transfer coefficient was set to 100 W/m^2K and the liquid temperature to 320 K. On solid-air boundaries, the heat-transfer coefficient was set to 50 W/m^2K and the air temperature to 290 K. On the boiling surface, the heat-transfer coefficient was set to 2090 W/m^2K and the fluid temperature to 320 K.

A typical temperature distribution from the simulations is shown in Fig. 4. This simulation was undertaken with the aluminium body exposed to the atmosphere and in direct contact with the flowing fluid. This simulation indicated that an applied heat flux of 100 kW/m^2 at the heater surface would produce a 31 kW/m^2 heat flux at the boiling surface. With only liquid flowing in the test loop, Fig. 1, temperature rises were measured across the test piece, allowing the heat gain to be estimated from the mass flow rate of liquid and the inlet and outlet temperatures. The gain in sensible heat confirmed the simulation results. Further simulations were undertaken to aid the design of the test section's insulation. This led to a 25 mm layer of insulating wool being placed on all external surfaces, with the exception of the viewing window required for visual observations, Fig. 2. Additionally, all internal fluid-aluminium surfaces were insulated with a 6 mm layer of PTFE. Simulations indicated that these changes would give a heat flux of 84 kW/m^2 at the boiling surface when a heat flux of 100 kW/m^2 was applied by the heater.

The heat flow from the heater to the test piece is proportional to the difference between the heater temperature, T_h, and the test-piece surface temperature, T_w. Data taken when the liquid outlet temperature was below the saturation

temperature, deduced from the outlet fluid pressure, were used to establish this relationship. The effective heat flux, q_{eff}, was determined from the ratio of increase in sensible heat of the liquid to the base area of the test-piece, and was correlated by

$$q_{eff} = 2.891(T_h - T_w) - 1.452 \quad (2)$$

where the heat flux is in kW/m^2 and the temperatures are in Kelvin. The constant term estimates the heat loss through the glass window. This corresponds to 3.63 W. A constant value is reasonable because the fluid temperature, and therefore the bulk of the test section temperatures, were close to the saturation temperature of R113 at atmospheric pressure. If the transmission efficiency is taken as the ratio of the effective heat flux to the heat flux applied by the heater, Eq. (2) led to transmission efficiencies of 58-90%, depending on the mass flux, with 85% being typical.

4. Data reduction

The working fluid, which had a liquid specific heat capacity of c_p, was delivered to the test piece in a sub-cooled state. The test-piece was therefore divided into two lengths, a single phase length, L_{sub}, and a boiling length, L_{sat}, as shown in Fig. 5. The fluid, which had a saturation temperature of T_{sat}, approached the test piece, of width W, at a temperature of T_{in} and at a mass flow rate of M. The length of the test piece in single-phase flow was therefore estimated from

$$L_{sub} = \frac{Mc_p(T_{sat} - T_{in})}{q_{eff}W} \quad (3)$$

Since the test piece had a length L, the boiling length was estimated from

$$L_{sat} = L - L_{sub} \quad (4)$$

A linear pressure distribution was assumed across the test piece. This was deduced from the measured inlet pressure, p_{in}, and the measured pressure drop, Δp. Thus,

$$p = p_{in} - \Delta p \frac{z}{L} \quad (5)$$

where z was the distance from the beginning of the test piece. The saturation temperature is a function of pressure. Thus, the saturation temperature at the onset of boiling was evaluated from the local pressure, p. The process was iterative.

For the pin-fin surface, the local heat transfer coefficient was obtained by separating the flow field into cells. A typical cell is shown in Fig. 6. This pattern existed parallel and perpendicular to the flow. There were two heat flow paths. The first was through the base of the test piece to the fluid and the second was through the fins to the fluid. These flow paths allowed the fin efficiency approach to be used. A one-dimensional heat balance through the bottom of the test piece gave

$$q_{eff}\left(W_{ch}+W_w\right)^2=\alpha\left(T_w-T_f\right)\left[\left(W_{ch}+W_w\right)^2-W_w^2+4\eta W_w H_{ch}\right] \quad (6)$$

where α is the heat-transfer coefficient, η is the fin efficiency and T_f is the fluid temperature. The size of the heights and widths in Eq. (6) are given in Table 1. Since thermocouples were located within the test piece, three close to the inlet and three close to the outlet, Eq. (6) allowed two local heat-transfer coefficients to be deduced for each heat and mass flux set.

W_w/mm	W_{ch}/mm	W_{cell}/mm	H_{w1}/mm	H_{ch}/mm	H_{tc}/mm	H_{w2}/mm	H_{w3}/mm	H_{cell}/mm
0.5	1.0	2.0	10.0	1.0	1.5	5.0	5.0	21.0

Table 1: Dimensions of heat transfer unit cell

The variation in the measured inlet and outlet wall temperatures was typically less than 1°C, but could, on occasion, be as large as 2°C. The wall temperature was therefore obtained by averaging the readings from the three wall temperatures near the test piece inlet and outlet to obtain T_{tc}, which was then corrected for depth from the plate surface, H_{tc}, through the one-dimensional heat conduction equation, i.e.

$$T_w=T_{tc}-\frac{q_{eff}H_{tc}}{k} \quad (7)$$

in which k is the thermal conductivity of copper. The fluid temperature was obtained from the test piece partition shown in Fig. 5. If the heat balance indicated that the fluid above each set of thermocouples was subcooled, the subcooled temperature was used. Otherwise the saturation temperature corresponding to the local pressure was used.

The fin efficiency was found by assuming that the fins could be treated as rods with no heat transfer from their tips, i.e.

$$\eta = \frac{\tanh(mH_{ch})}{mH_{ch}} \tag{8}$$

where m was the fin parameter, given by

$$m = \sqrt{\frac{4\alpha}{kW_w}} \tag{9}$$

Thus, the process of obtaining the heat-transfer coefficient was iterative.

For the plate surface, the heat-transfer coefficient was found from

$$\alpha = \frac{q_{eff}}{(T_w - T_f)} \tag{10}$$

The local gas-mass fraction, x, was estimated from

$$x = \frac{q_{eff} W (z - L_{sub})}{M h_{fg}} \tag{11}$$

where h_{fg} is the enthalpy of evaporation.

5. Experimental results for single-phase flows

Heat-transfer coefficients and pressure drop measurements were obtained for single-phase liquid R113 near atmospheric pressure and temperature. For the pin-fin surface, heat-transfer coefficients were obtained for heat loads in the range 25-140 W. The heat load was chosen to give a rise in fluid temperature of at least 5 K. This gave apparent heat fluxes in the range 5-50 kW/m^2, based on the base area of the test plates. Five equally spaced mass flow rates between 2.5 g/s and 12.5 g/s were used. This gave mass fluxes in the range 50-250 kg/m^{2}s, based on the unrestricted flow area in the test channels. Pressure drops were obtained under isothermal conditions for the same mass fluxes. For the plate tests, the same mass flux range was used. However, the plate had a smaller heat-transfer area than the pin-fin surface. Thus, for the same heat flux, the wall temperature was higher. Lower heat fluxes were therefore applied during the plate tests to prevent excessive temperatures in the heater.

The single-phase heat-transfer coefficients are shown for the range of mass fluxes in Fig. 7. The estimated error in the heat-transfer coefficient is ±10%. The heat-transfer coefficients at the inlet and outlet positions of the plate are shown to be similar in magnitude and to increase with increasing mass flux. The pin-fin inlet and outlet values are shown to be different in magnitude, with both following a power law function of the mass flux. Since the plate data approximately follow a single curve and the pin-fin data do not, and with the inlet data corresponding to the 7^{th} row of pin fins and the outlet to the 19^{th}, the difference is probably a settling length effect caused by the pin-fins.

The variation of single-phase pressure drop with mass flux is shown for the pin-fin surface in Fig. 8. The pressure drop is shown to be a power law function of the mass flux, as would be expected. The plate pressure drops were too small to be measured by the pressure transducer.

6. Experimental results for the two-phase flows

The two-phase tests were performed by supplying liquid R113 near atmospheric pressure to the test section with 2-5 K of subcooling. Heat-transfer and pressure drop data were obtained for heat loads in the range 25-400 W. These were applied to each mass flow rate in steps of 25 W, with the 375 W load avoided. This gave apparent heat fluxes in the range 10-160 kW/m^2. The five mass flow rates used in the single-phase tests were used for each heat flux. For the plate surface at the lower mass fluxes, some of the larger heat fluxes were not possible, as damage to the electrical heater would have resulted from the excessive temperatures generated by the reduced heat-transfer area available relative to the pin-fin case.

The experimental procedure for these tests led to the occurrence of three types of heat-transfer, single-phase, subcooled boiling and saturated boiling. Single-phase heat-transfer was taken to have occurred when the fluid above the thermocouple was in a subcooled state and the wall temperature was below the local saturation value. Subcooled boiling heat-transfer was taken to have occurred when the fluid above the thermocouple was in a subcooled state and the wall temperature was above the local saturation value. Saturated boiling heat-

transfer was taken to have occurred when the fluid above the thermocouple was in a saturated state and the wall temperature was above the local saturation value.

The variation of the measured heat-transfer coefficients with the effective heat fluxes are shown for each mass flux in Fig. 9. The test-piece wall thermocouples were located 12.5 and 37.5 mm from the test pieces' inlets. Inlet and outlet heat-transfer coefficients refer respectively to the 12.5 and 37.5 mm locations. In general, the pin-fin surface was subjected to all three heat transfer types. The plate had a smaller heat-transfer surface than the pin-fins. Thus, for the same heat flux, the wall temperatures were higher; giving only subcooled and saturated boiling heat transfer on the plate surface.

6.1 Heat-transfer at a mass flux of 50 kg/m^{2}s

The heat-transfer coefficient variation for the lowest mass flux of 50 kg/m^{2}s is shown in Fig. 9a. For the pin-fin surface, single-phase convection occurs at both the inlet and outlet locations at a heat flux of approximately 6 kW/m^2. The inlet and outlet values are not the same, as discussed in Section 5. In the heat flux range of 16-35 kW/m^2, the inlet heat-transfer coefficient is shown to rise from levels below the outlet values to the outlet value. Within this range, the inlet flow is shown to be in the subcooled boiling regime. Thus, the merging of the heat-transfer coefficients is consistent with the single-phase settling length being longer that the two-phase equivalent. At heat fluxes in the range 35-60 kW/m^2, the inlet and outlet heat-transfer coefficients are shown to be similar in magnitude, in the saturated boiling regime and independent of heat flux. At heat fluxes greater than 60 kW/m^2 the inlet and outlet heat-transfer coefficients are again similar in magnitude and in the saturated boiling regime. However, they are not independent of heat flux. The gas-mass fractions at the inlet and outlet locations are approximately 0.03 and 0.19 respectively at a heat flux of 45 kW/m^2 and 0.2 and 0.68 respectively at a heat flux of 136 kW/m^2. Thus, the saturated boiling heat-transfer coefficients are independent of gas-mass fraction. For the plate surface, subcooled boiling is shown to exist at the inlet location for heat fluxes in the range 6-25 kW/m^2, with saturated boiling occurring thereafter. Saturated boiling is shown to occur for all heat fluxes at the plate outlet. The merging characteristic of the plate is similar to that obtained with the pin-fin surface up to a heat flux of 65 kW/m^2, where the increasing characteristic is not achieved. Instead, a reasonably constant value is maintained until a heat flux of

approximately 80 kW/m^2 is achieved, after this a dip occurs. Fig. 10 shows typical observed flow patterns for the pin-fin and plate surfaces at a heat flux of 80 kW/m^2. The pin-fin surface contains small bubbles moving between the pins, Fig. 10a. The plate surface contains dried out areas covering relatively large areas, Figs. 10b, 10c. These dried out areas appeared at lower heat fluxes and grew in size and dominance until the plate surface heat-transfer coefficient decreased at a heat flux of around 75 kW/m^2. It is possible that the drop in heat-transfer coefficient for the pin-fin surface at 140 kW/m^2 is also associated with dryout.

6.2 Heat-transfer at mass fluxes greater than 50 kg/m^{2}s

For both surfaces, as the mass flux increases, Figs. 9b-9e, the number of inlet points in the subcooled boiling region increases. At mass fluxes of 150 kg/m^{2}s and above, an increasing number of the outlet points are also in this regime, Figs. 9c-9e. This results from the increased amount of absolute sensible enthalpy change that is required to reach saturation as a consequence of the mass flux increase. At these larger mass fluxes, the description given for Fig. 9a is, in the main, repeated. There are two major differences. Firstly, the region where the heat-transfer coefficient is reasonably independent of heat flux decreases as the mass flux increases, and secondly, for the pin-fin surface at a mass flux of 250 kg/m^{2}s, the outlet subcooled boiling heat-transfer coefficient over-shoots the saturated boiling value. The range of gas-mass fractions is reduced at the larger mass fluxes, but the saturated boiling heat-transfer coefficient remains independent of it.

6.3 Heat-transfer mechanism

All of the saturated boiling data identified in Figs. 9a-9e are reproduced in Fig. 11. The pin-fin data, Fig. 11a, are reasonably independent of location and mass flux and follow the power law relationship

$$\alpha = 0.869 q_{act}^{0.398} \tag{12}$$

to within ±10% of the measured values. Equation (12) is based on the actual heat flux, q_{act}, i.e. the heat flux based on the actual heat-transfer area. The plate data, Fig. 11b, behave similarly, following the power law relationship

$$\alpha = 0.557 q_{eff}^{0.467} \tag{13}$$

In this case the actual and effective heat fluxes are the same. It therefore seems likely that the dominating heat-transfer mechanism in the saturated boiling flow regime for both surfaces is the nucleate boiling regime.

The plate power law is included in Fig. 11a and the pin-fin law in Fig. 11b. Both data sets are similar in magnitude, with the pin-fin values being slightly higher. This indicates that the pin-fin surface improves heat transfer by increasing the surface area and the heat-transfer coefficient.

6.3 Two-phase pressure drop

The variation of two-phase pressure drop with heat flux for a range of mass fluxes is shown in Fig. 12. The pin-fin pressure drop is shown to increase with increasing heat flux. For all but the highest mass flux, the pressure drop is also shown to increase with mass flux. There are two opposing effects that could cause this to occur. The first is that pressure drop increases with increasing mass flux. The second is that the pressure drop increases with increasing vapour content. For the same heat flux, as the mass flux increases, the vapour content decreases, leading to the trends shown in Fig. 12. The plate data is shown to be reasonably proportional to heat flux and to be considerably smaller than the pin-fin data by a factor of about 7.

7. Analysis

The pin-fin surface geometry has some similarities with tube bundles. The similarity has limitations. In particular, the length to diameter ratio is much larger in tube bundles than in this pin-fin arrangement. None-the-less, the data were compared to tube bundle methods to evaluate if macro-scale knowledge of this type is transferable to this length scale. To do this, the equivalent diameter for a square pin was chosen to give the same circumference as an equivalent circular tube.

7.1 Single-phase flow comparisons

For the pin-fin geometry, predictions from the single-phase heat-transfer coefficient method of ESDU (1973) and from the pressure-drop method of ESDU (1979) are included in Figs. 7 and 8 respectively. The predictions of the inlet and outlet heat-transfer coefficient differ because they are row dependent. The agreement between the measured and the predicted heat-transfer coefficient is not too bad, indicating that correlations for these surfaces may be informed by macro-scale know-how. The agreement between the measured and the predicted pressure drops is reasonable. However, more geometrical variations would need to be tested before its applicability can be considered general.

For the plate surface, Ansys CFX 11 was used to deduce the heat-transfer coefficient. A two-dimensional simulation of a channel 70 mm long and 1 mm high was simulated. This allowed the 20 mm of settling length upstream of the plate to be included. A uniform velocity inlet was assumed along with a constant pressure exit. The mesh size was systematically halved until the solution was independent of grid size. Temperature dependent fluid properties were used. The resultant predicted heat-transfer coefficients are included in Fig. 7. The agreement is reasonable.

7.2 Two-phase heat-transfer comparisons

A comparison of the two-phase heat-transfer data with the nucleate pool boiling correlations of Mostinski (1963) and Cooper (1984) is included in Fig. 9. The surface roughness parameter was chosen to remove the surface roughness dependency from the Cooper (1984) prediction. For all mass fluxes and both surfaces, the Mostinski (1963) correlation lies below the measured values and the Cooper (1984) agrees reasonably well. Given the uncertainty in predicting nucleate pool boiling, this is a reasonable comparison and is further evidence that the heat-transfer process is dominated by nucleate boiling.

For the pin-fin surface, predictions of the saturated boiling heat-transfer coefficient were obtained from tube bundle methods thus

$$\alpha = S\alpha_{nb} + F\alpha_c \tag{14}$$

where α_{nb} is the nucleate boiling heat-transfer coefficient, obtained from the method of Mostinski (1963), α_c is the single-phase, convective, heat-transfer coefficient, obtained from the method of ESDU (1973) by assuming that only the liquid component flowed in the heat exchanger, S is the nucleate boiling suppression factor, obtained from the method of Bennet et al (1980) and F is the convective enhancement factor, given by

$$F = \left(\phi_l^2\right)^{0.36} \tag{15}$$

where the two-phase multiplier, ϕ_l^2, was obtained from Ishihara et al (1980), i.e.

$$\phi_l^2 = 1 + \frac{8}{X_{tt}} + \frac{1}{X_{tt}^2} \tag{16}$$

The predictions from Eq. (14) are included in Fig. 9. The comparison with the experimental data shows that the predictions for the inlet conditions are in reasonable agreement with the measured values at the inlet and outlet. This

results from the nucleate suppression of Mostinski (1963) balancing with the convective enhancement of ESDU (1973). However, the outlet predictions are significantly larger than the measured outlet values. Since the outlet gas mass-fraction is significantly larger than the inlet value, the difference between the inlet and outlet predictions is due to convective enhancement. Thus the measured data are consistent with convective enhancement not occurring for this geometry, again supporting nucleate boiling domination.

7.3 Two-phase pressure-drop comparisons

Two-phase pressure drops are predicted for horizontal flows from the simultaneous integration of the pressure gradient, *dp/dz*, given by

$$\frac{dp}{dz} = \left(\frac{dp}{dz}\right)_A + \left(\frac{dp}{dz}\right)_F \qquad (17)$$

where $(dp/dz)_A$ is the pressure gradient due to acceleration and $(dp/dz)_F$ is the pressure gradient due to friction, and the energy equation, the differential form of Eqn. (11). This approach allows the variation of physical properties to be included. The acceleration pressure gradient was determined by assuming homogeneous flow. For the pin-fin surface, the frictional pressure gradient was obtained from the two-phase multiplier method of Ishihara et al (1980), Eqn. (16) with the liquid-only single-phase pressure drops obtained from ESDU (1979). For the plate surface, the two-phase multiplier was obtained from Chisholm (1983), with the single-phase pressure gradient found from laminar channel flow theory. The Chisholm (1983) method is similar to Eqn (16), with coefficient 8 replaced by a value that depends on whether the vapour and liquid phases are in the laminar or turbulent flow regime. The predictions are included in Fig. 12. For the pin-fin surface the agreement between the measured and predicted values is reasonable. The acceleration component never accounts for more than 15% of the total. Thus, the friction method of Ishihara et al (1980) is shown to be reasonable. For the plate surface the agreement between the measured and predicted values is also reasonable. However, these predictions are dominated by acceleration, accounting for up to 70% of the total.

8. Conclusions

Heat-transfer and pressure drop data have been obtained for pin-fin and plate geometries. The two-phase heat-transfer coefficient for the pin-fin surface is similar in magnitude to that for the plate. However, the pin-fin surface

area is 70% larger and the heat-transfer coefficient is slightly larger, allowing a much lower surface temperature for the same heat flux. Thus, pin-fin surfaces improve the heat transfer by increasing the heat-transfer surface and the heat-transfer coefficient. The pressure drop in the pin-fin surface is about seven times larger than that for the plate. Thus, the reduction in wall temperature is achieved by a significant pressure drop penalty. The pin-fin data have also been compared to macro-scale design methods. These show that macro-scale heat-transfer may aid the selection of correlating parameters for pin-fin surfaces and that pressure drop methods may be transferable, although more surfaces will need to be tested before this can be stated conclusively. The data and the predictions suggest that heat-transfer is heat flux dependent and that convective enhancement does not occur on the pin-fin surface. These data were obtained for R113 and are therefore likely to be applicable to more readily available fluids such as FC72.

Nomenclature

C_o	confinement number
c_p	specific heat at constant pressure
D_h	hydraulic diameter
F	convective enhancement factor
g	acceleration due to gravity
h_{fg}	enthalpy of evaporation
H	test-piece heights (see Table 1)
k	thermal conductivity
L	test-piece lengths
m	fin parameter
M	mass flow rate
p	pressure
q_{eff}	effective heat flux
S	nucleate boiling suppression factor
T	temperature
W	test-piece widths (see Table 1)

Greek characters

α	heat-transfer coefficient
Δp	pressure drop
ρ	density
σ	surface tension
ϕ_l^2	two-phase multiplier
η	fin efficiency

Subscripts

c	convective
f	fluid value
h	at the heater
in	inlet value
L	liquid phase
nb	nucleate boiling
sat	saturated value
sub	subcooled value
tc	at thermocouple location

X	Martinelli parameter	*tt*	turbulent vapour and turbulent liquid
z	distance from test-piece inlet	*v*	vapour phase
		vv	viscous vapour and viscous liquid
		w	wall value

Acknowledgements

The authors would like to thank the EPSRC who financed this work through grant EPSRC EP/D500117/1**.**

References

Z. Y. Bao, D. F. Fletcher and B. S. Haynes, 2000, Flow boiling heat transfer of Freon R11 and HCFC123 in narrow passages, Int. J. Heat Mass Transfer, Vol. 43, pp. 3347–3358.

J. Barber, K. Sefiane, D. Brutin and L. Tadrist, 2009, Hydrodynamics and heat transfer during flow boiling instabilities in a single microchannel, Applied Thermal Engineering, Vol. 29, pp. 1299–1308.

D. L. Bennett, M. W. Davis and B. L. Hertzler, 1980, The suppression of saturated nucleate boiling by forced convective flow, AIChE Symp. Ser. Vol. 26, pp. 91-103.

D. Bogojevic, K. Sefiane, A.J. Walton, H. Lin, and G. Cummins, 2009, Two-phase flow instabilities in a silicon microchannels heat sink, International Journal of Heat and Fluid Flow, In Press, Available online 1 May 2009.

D. Chisholm, 1983, Two-phase flow in pipelines and heat exchangers. George Goodwin, London and New York.

M. G. Cooper, 1984, Heat flow rates in saturated nucleate pool boiling – A wide ranging examination using reduced properties, Advances in Heat Transfer, Academic press, Orlando, Vol. 16, pp 157-239.

R. Dowlati, M. Kawaji and A. M. C. Chan, 1990, Pitch-to-Diameter Effect on Two-Phase Flow across an in-Line Tube Bundle, AIChE Journal, Vol. 36, pp. 765-772.

R. Dowlati, A. M. C. Chan and M. Kawaji, 1992, Hydrodynamics of Two-Phase Flow across Horizontal in-Line and Staggered Rod Bundles, Journal of Fluids Engineering, Transactions of the ASME, Vol. 114, pp. 450-456.

ESDU, 1973, Convective heat transfer during crossflow of fluids over plain tube banks, Vol. 73031.

ESDU, 1979, Crossflow Pressure Loss over Banks of Plain Tubes in Square and Triangular Arrays Including Effects of Flow Direction, Engineering Sciences Data Unit, Vol. 79034, pp. 17.

A. Feenstra, D. S. Weaver and R. L. Judd, 2000, Improved Void Fraction Model for Two-Phase Cross-Flow in Horizontal Tube Bundles, International Journal of Multiphase Flow, Vol. 26, pp. 1851-1873.

H. Honda, H. Takamastu and J. J. Wei, 2002, Enhanced boiling of FC-72 on silicon chips with micro-pin-fins and submicron-scale roughness, J Heat Transfer, Vol. 124, pp 383-390.

H. Honda and J. J. Wei, 2004, Enhanced boiling heat transfer from electronic components by use of surface microstructures, Experimental Thermal and Fluid Sciences, Vol. 28, pp 159-169.

G. Hetsroni, A. Mosyak, Z. Segal and E. Pogrebnyak, 2003. Two-phase flow patterns in parallel micro-channels. Int. J. Multiphase Flow Vol. 29, pp. 341–360.

K. Ishihara, J. W. Palen and J. Taborek, 1980, Critical Review of Correlations for Predicting Two-Phase Flow Pressure Drop across Tube Banks, Heat Transfer Engineering, Vol. 1, pp. 23-32.

S. G. Kandlikar, 2001, Two-phase flow patterns, pressure drop and heat transfer during boiling in mini-channel and micro-channel flow passages of compact heat exchangers. In: Compact Heat Exchangers and Enhancement Technology for the Process Industries, Begell House, New York, pp. 319-334.

S. G. Kandlikar and M.E. Steinke, 2002, Flow Boiling Heat Transfer Coefficient in Minichannels – Correlation and Trends. Proceedings of 12th International Heat Transfer Conference, Grenoble, France, Paper 1178.

P.A. Kew and K. Cornwell, 1996, On pressure fluctuations during boiling in narrow channels, 2nd European Thermal-Science and 14th UIT National Heat Transfer Conference, Rome, pp. 1323–1327.

P. A. Kew, and K. Cornwell, 1997, Correlations for Prediction of Boiling Heat Transfer in Small-Diameter Channels, Applied Thermal Engineering, Vol. 17, pp. 705-715.

P. A. Kew, E. Adom and K. Cornwell, Heat flux controlled boiling in confined spaces, 13th International Heat Transfer Conference, Sydney, 2006.

A. Kosar and Y. Peles, 2007, Boiling heat transfer in a hydrofoil-based micro pin fin heat sink, Int J Heat and Mass Transfer, Vol. 50, pp 1018-1034.

A. Kosar, 2008, Two-phase pressure drop across a hydrofoil-based micro pin device using R-123, Experimental Thermal and Fluid Science, Vol. 32, pp 1213-1221.

S. Krishnamurthy and Y. Peles, 2008, Flow boiling of water in a circular staggered micro-pin fin heat sink, Int J Heat and Mass Transfer, Vol. 51, 1349-1364.

S. Krishnamurthy and Y. Peles, 2009, Surface tension effects on adiabatic gas-liquid flow across micro pillars, Int J Multiphase flow, Vol. 35, pp 55-65.

S. Krishnamurthy and Y. Peles, 2007, Gas-liquid two-phase flow across a bank of micro pillars, Phys Fluids, Vol. 19, pp. 43302-43314.

G.M. Lazarek and S.H. Black, 1982, Evaporative heat transfer, pressure drop and critical heat flux in a small vertical tube with R-113, Int. J. Heat Mass Transfer Vol. 25, pp. 945–960.

Y. M. Lie, J. H. Ke, W. R. Chang, T. C. Cheng and T. F. Lin, 2007, Saturated flow boiling heat transfer and associated bubble characteristics of FC-72 on a heated micro-pin finned silicon chip, Int J Heat and Mass Transfer, Vol. 50, pp 3862-3876.

S. Lin, P.A. Kew and K. Cornwell, 2001, Two-phase heat transfer to a refrigerant in a 1 mm diameter tube, Int. J. Refrigeration, Vol. 24, pp. 51–56.

A. Ma, J. Wei, M. Yuan and J. Fang, 2009, Enhanced flow boiling heat transfer of FC-72 on micro-pin-finned surfaces, Int J Heat and Mass Transfer, Vol. 52, pp 2925-2931.

S. S. Mehendal, A. M. Jacobi and R. K. Shah, 2000, Fluid flow and heat transfer at micro- and meso-scales with application to heat exchanger design, Appl. Mech. Rev. Vol. 53, pp. 175-193.

I. L. Mostinski, 1963, Calculation of heat transfer and critical heat flux in boiling liquids based on law of corresponding states. Teploenergetika, Vol. 10, pp 66-71.

W. Qu and A. Siu-Ho, 2009, Experimental study of saturated boiling heat transfer in an array of staggered micro-pin-fins, Int J Heat and Mass Transfer, Vol. 52, pp 1853-1863.

F. H. Rahman, J. G. Gebbie and M. K. Jensen, 1996, Interfacial Friction Correlation for Shell-Side Vertical Two-Phase Cross-Flow Past Horizontal in-Line and Staggered Tube Bundles, International Journal of Multiphase Flow, Vol. 22, pp. 753-766.

D. S. Schrage, J. T. Hsu and M. K. Jensen, 1988, Two-Phase Pressure Drop in Vertical Crossflow across a Horizontal Tube Bundle, AIChE Journal, Vol. 34, pp. 107-115.

D. Shiferaw, T. G. Karayiannis and D. B. R. Kenning, 2009, Flow boiling in a 1.1 mm tube with R134a: Experimental results and comparison with model, International Journal of Thermal Sciences, Vol. 48, pp. 331-341.

J. R. Thome, V. Dupont and A. M. Jacobi, 2004, Heat transfer model for evaporation in microchannels, Part I: presentation of the model, Int.J. Heat Mass Transfer 47, pp. 3375–3385.

T. N. Tran, M. W. Wambsganss and D. M. France, 1996, Small circular- and rectangular-channel boiling with two refrigerants, Int. J. Multiphase Flow, Vol. 22, pp. 485–498.

M. W. Wambsganss, D. M. France, J. A. Jendrzejczyk, T. N. Tran, 1993, Boiling heat transfer in a small-diameter tube, J. Heat Transfer Vol. 115, pp. 963–972.

G. Wang, P. Cheng, H. Wu, 2007, Unstable and stable flow boiling in parallel microchannels and in a single microchannel, International Journal of Heat and Mass Transfer, Vol. 50, pp. 4297-4310.

J. Xu, J. Zhou, Y. Gan, 2005, Static and dynamic flow instability of a parallel microchannel heat sink at high heat fluxes, Energy Conversion and Management, Vol. 46, pp. 313-334.

Y. Yan and D. B. R. Kenning, 1998, Pressure and temperature fluctuations during boiling in narrow channel, Eurotherm 62: Heat Transfer Condensation Evaporation, Grenoble pp. 107–1223.

M. Yuan, J. Wei, Y. Xue and J. Fang, 2009, Subcooled flow boiling heat transfer of FC-72 from silicon chips fabricated with micro-pin-fins., Int J Thermal Sciences, Vol. 48, pp 1416-1422.

W. Zhang, T. Hibiki, and K. Mishima, 2004,Correlation for flow boiling heat transfer in mini-channels, Int J Heat Mass Transfer, Vol. 47, pp. 5749-5763.

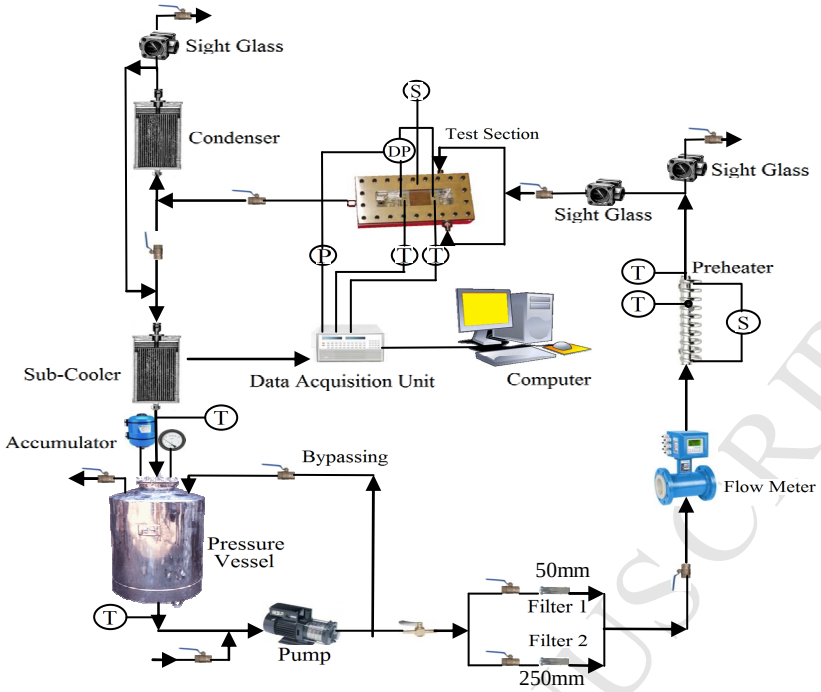

Figure 1: Flow loop

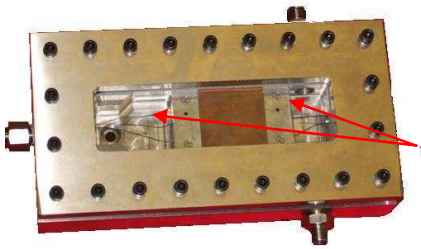

Figure 2a; top view-pre-insulation

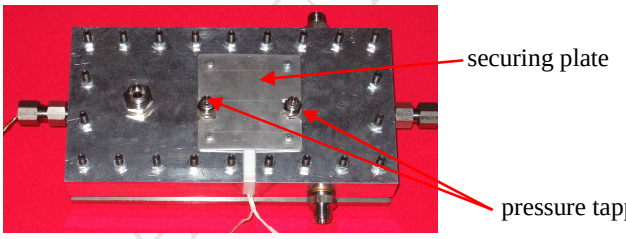

Figure 2b: bottom view-pre-insulation

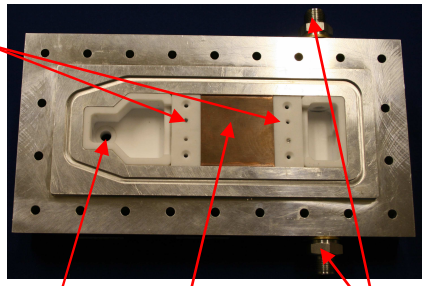

Figure 2c: open view with internal insulation

Figure 2: test section

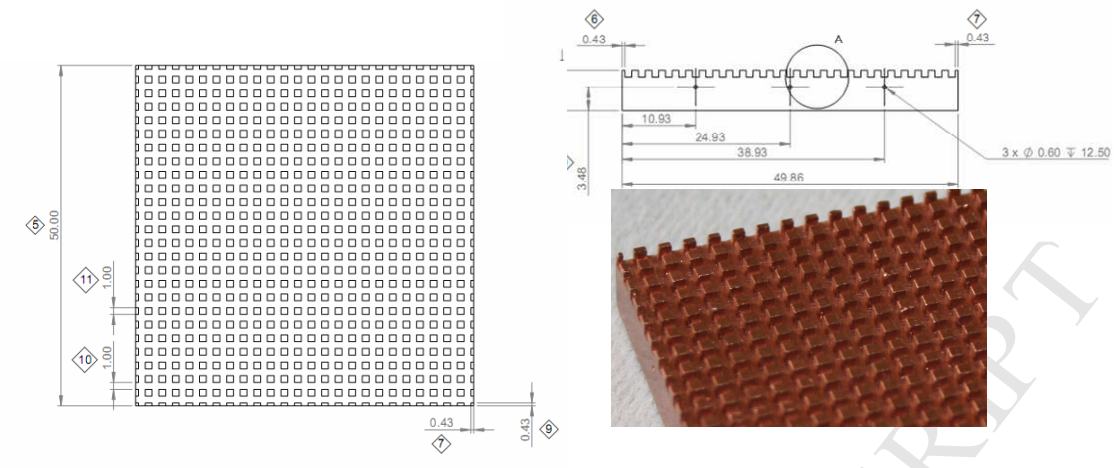

Figure 3: Test piece

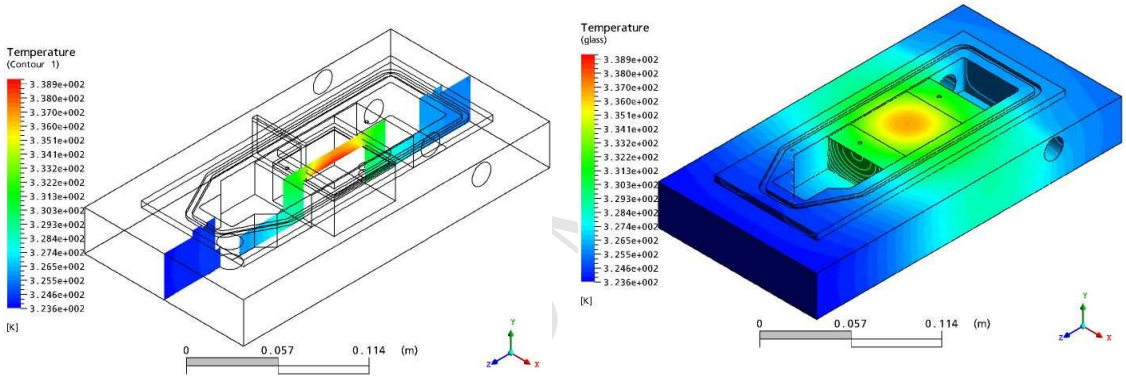

Figure 4: Predicted temperature distribution without insulation

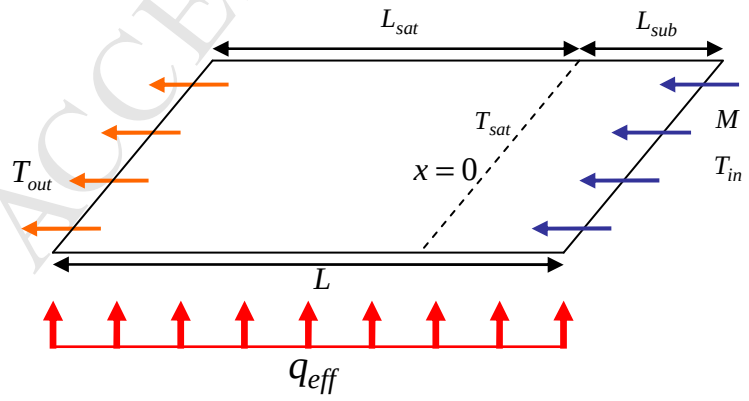

Figure 5: Heat load partition

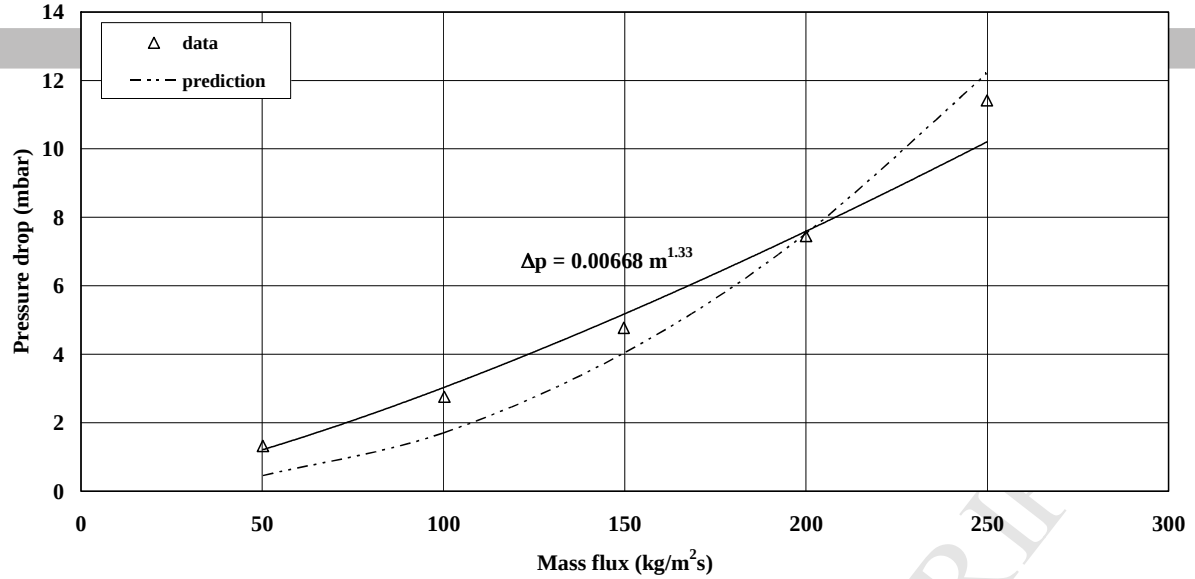

Figure 8: Variation of single-phase pressure drop with mass flux

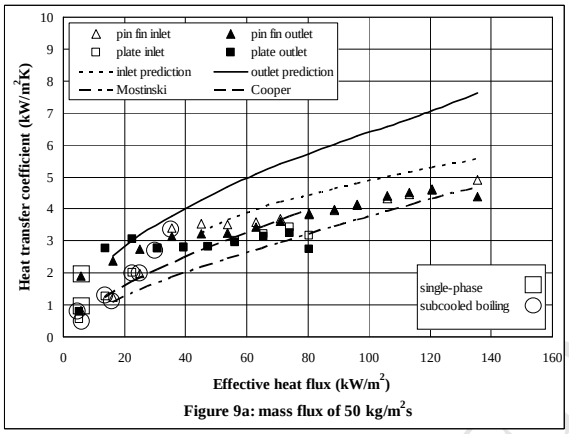

Figure 9a: mass flux of 50 kg/m²s

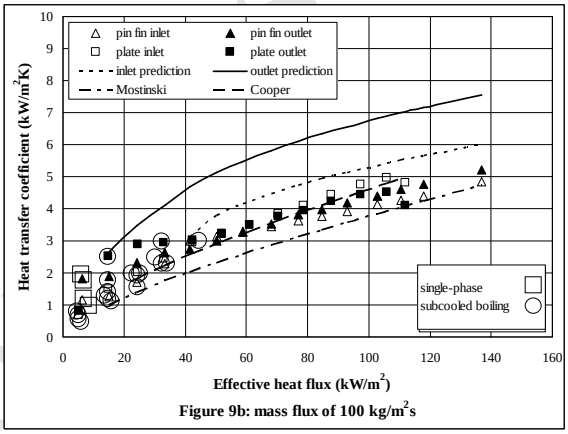

Figure 9b: mass flux of 100 kg/m²s

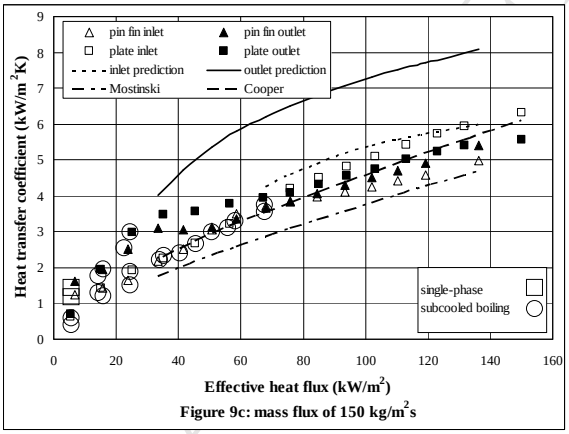

Figure 9c: mass flux of 150 kg/m²s

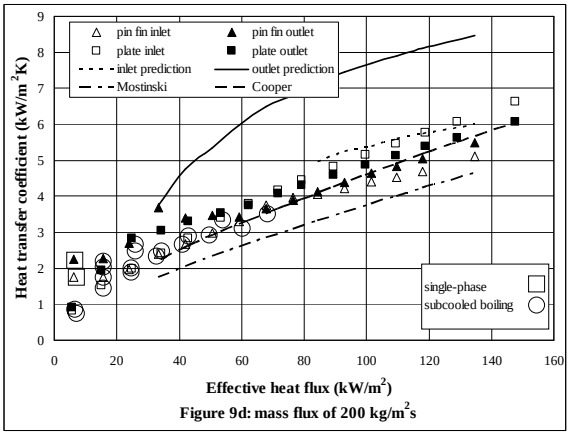

Figure 9d: mass flux of 200 kg/m²s

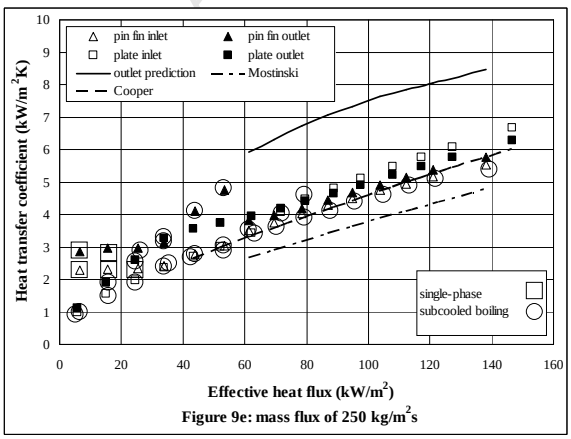

Figure 9e: mass flux of 250 kg/m²s

Figure 9: Variation of heat-transfer coefficient with effective heat flux for a range of mass fluxes

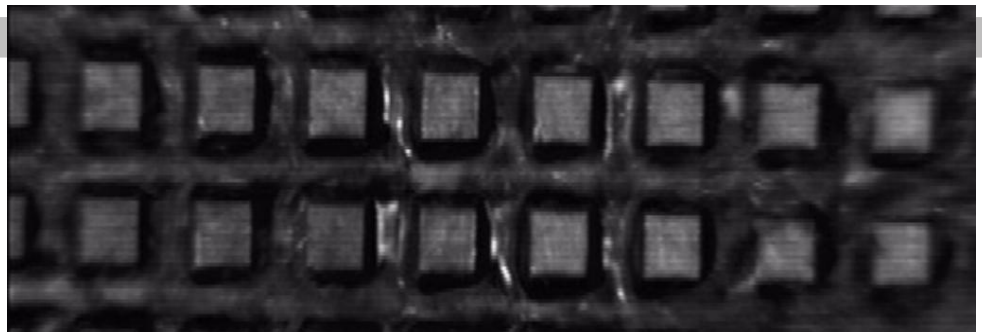

Figure 10a: pin-fin surface

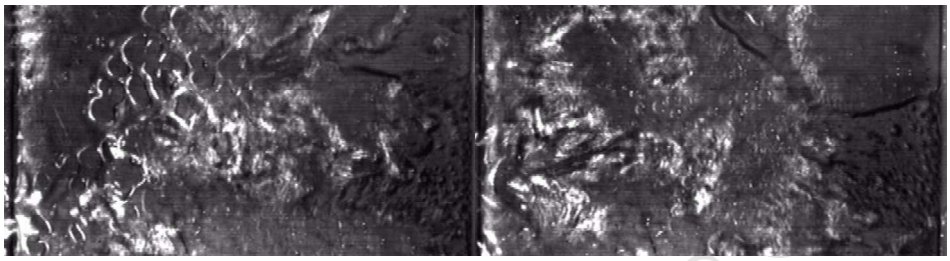

Figure 10b: plate surface

Figure 10c: plate surface

Figure 10: Typical views of the flow at a heat flux of 80 kW/m^2

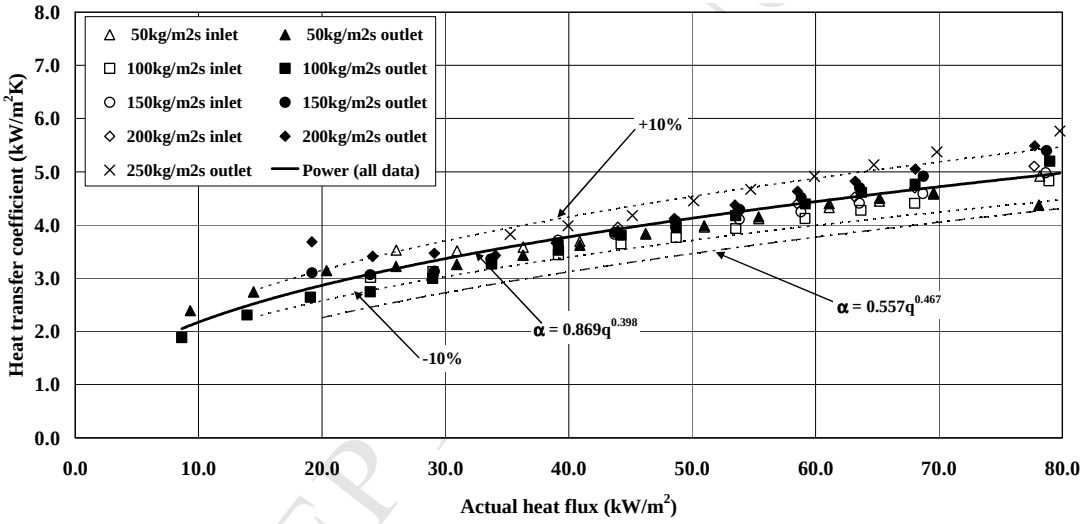

Figure 11a: pin-fin surface

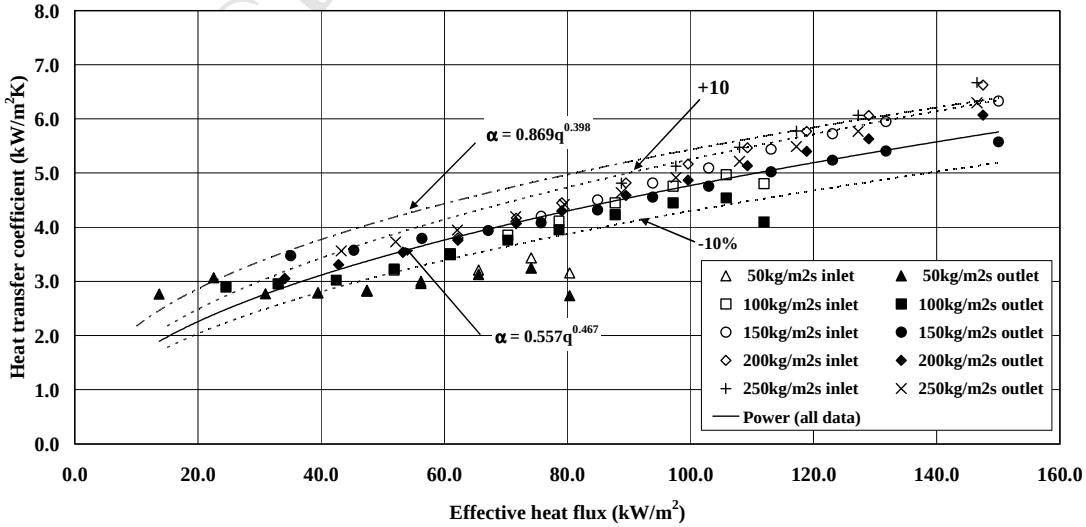

Figure 11b: Plate surface

Figure 11: Variation of saturated boiling heat-transfer coefficient with actual heat flux

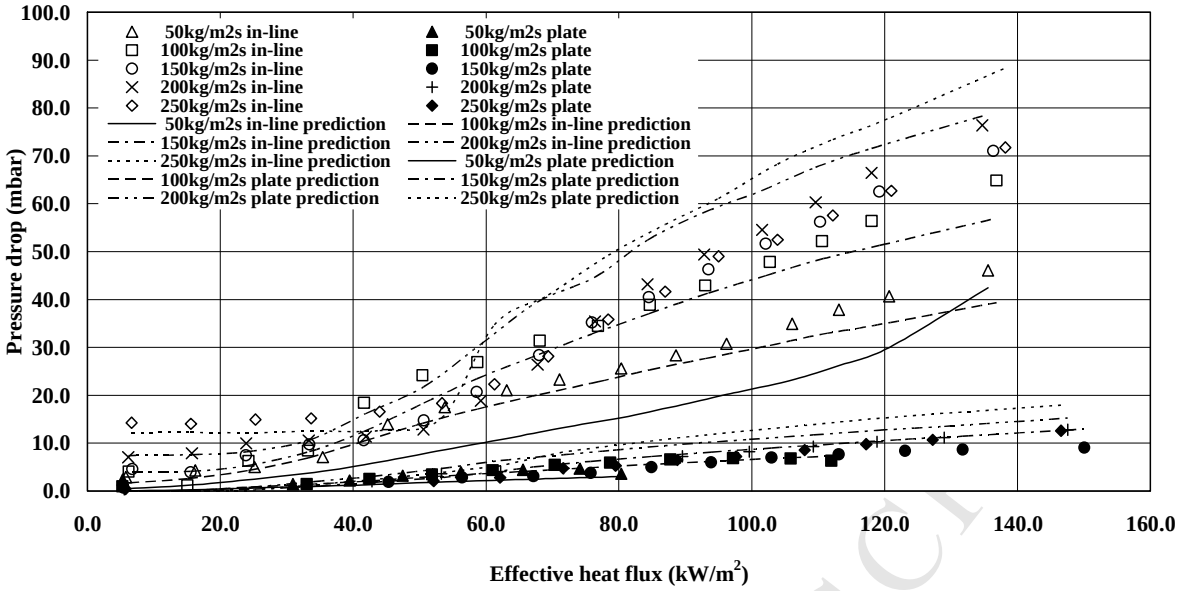

Figure 12: Variation of pressure drop with effective heat flux at various mass fluxes